Uncertainty in LAI and Fractional Cover Estimation from Airborne Imagery: Effects of Viewing Geometry and Positional Uncertainty in the Case of Barrax SPARC Campaign

CHRISTABEL TENDAI TANDIWE MAGUMA
[May, 2012]

SUPERVISORS:
M.Sc. V. Venus (First Supervisor)
Prof. Dr. Ing. W. Verhoef (Second Supervisor)

Uncertainty in LAI and Fractional cover estimation from Airborne Imagery; effects of viewing geometry and positional uncertainty in the case of Barrax SPARC campaign

CHRISTABEL TENDAI TANDIWE MAGUMA
Enschede, the Netherlands, [February, 2012]

Thesis submitted to the Faculty of Geo-Information Science and Earth Observation of the University of Twente in partial fulfilment of the requirements for the degree of Master of Science in Geo-information Science and Earth Observation.
Specialization: Natural Resources Management

SUPERVISORS:
M.Sc. V. Venus (First Supervisor)
Prof. Dr. Ing. W. Verhoef (Second Supervisor)

THESIS ASSESSMENT BOARD:
Dr. Y. A. Hussin (Chair)
Dr. Ir. C. v d Tol (External Examiner, ITC)

DISCLAIMER

This document describes work undertaken as part of a programme of study at the Faculty of Geo-Information Science and Earth Observation of the University of Twente. All views and opinions expressed therein remain the sole responsibility of the author, and do not necessarily represent those of the Faculty.

ABSTRACT

The purpose for this paper is to present a method using remote sensing measurement for improved retrieval of Leaf Area Index and fractional cover as input in the Surface Energy Balance Systems model. The method for estimation is based on comparing LAI based on the empirical relationship between LAI and vegetation Indices (NDVI) against Beer's law derivative for LAI and Poisson derived model for factional cover estimation. Furthermore the influenced of correcting satellite data by accounting for the variability in the viewing angle is investigated. In comparison to the ground observation, both SEBS automated routine and Beer's law derivative model under predicted LAI and thus exhibited a relatively weak predicting power on both the ASTER and the AHS data. The Aster data however showed a better R^2 0.6249 and 0.6004 for the SEBS routines and the Beer's law derivative model respectively with the scatter produced on the Aster data by the Beer's law derivative model representing results more closely to the ground data. For fractional cover estimation subtle difference in the models' estimation was observed with the major difference being observed at higher values of the viewing angle. Statistically the major difference is based on the R^2 (0.94) and the RMSE of the Poisson model derivative parameterization that showed the model performed better when multiplied by the cosine of the viewing zenith angle. This study is site specific and is achieved based on aircraft, satellite and field measurements made at the Barrax Agriculture Study Site in Spain during the SPARC campaign in 2004.

ACKNOWLEDGEMENTS

The success of this study is attributed to the collective effort and support of various people. I give my sincere gratitude to my first supervisor Valentijn Venus MSc whose guidance, patience and encouragement gave me the confidence to execute this research work. I am grateful to my second supervisor Professor Dr. Ing. Wouter Verhoef for his input. My sincere gratitude also goes to Professor Bob Su for providing the bulk of the data used in this study and the French team for providing the LAI measurements. I'm also indebted to Wim Timmermans, Dr Joris Timmermans and Dr Hans van der Kwast for answering my questions and all the assistance they gave to me.

I am also very deeply grateful to the Netherlands Fellowship Programme (NUFFIC) for affording me an opportunity to pursue this MSc degree. Special thanks goes to the course coordinator Dr Michael Weir, professors, lecturers and support staff of the NRM course for the support throughout my study period. I want to also appreciate the participants of the 2010-2012 NRM courses for the collaborations and the quality time we have shared. Furthermore i also extend my gratitude and thanks to my fellow countrymen for being my second family and providing the support and encouragement I needed. Finally I want to thank my family for being at the centre of my support system and I would like to give glory and honour to God for bringing me this far.

TABLE OF CONTENTS

LIST OF FIGURES

LIST OF TABLES

1. INTRODUCTION

1.1. Background

There is a growing concern over the ability of agriculture to support increasing populations such that the eradication of poverty and hunger was included as goal one of the United Nations Millennium Development Goals that were adopted in 2000 (Rosegrant *et al.*, 2003). Global food insecurity together with the continually growing population and consumption for food is expected to remain a worldwide concern for at least another 40years and beyond (Godfray *et al.,* 2010).

According to Wilhite *et al* (2007) drought is key threat to this global food security and it is a gradual, slow-onset natural hazard whose impact goes beyond the degree of direct exposure to or frequency of drought itself, but also by indirectly affecting dynamic responses to changes in the economic, social and environmental characteristics of the region. This amounts to drought contributing to great losses to agricultural production and recently crop yield has fallen because of declining investments in research and infrastructure, as well as increasing water scarcity (Rosegrant & Cline, 2003). Wilhite (2007) states that this has prompted an increasing need for measures to reduce the impacts of drought on agriculture and other sectors as well as an increase in demand for government or donor-sponsored assistance programs. A major research challenge is to develop suitable techniques for the forecasting the onset and termination of droughts (Mishra *et al.*, 2011).

Drought monitoring systems can be set up to enable advance warning to farmers and agriculture managers since drought at a critical stage during crop growth has an impact on yield. Satellite data has therefore become popular in the detection and occurrences of drought. Vegetation indices such as (Normalized Difference Vegetation Index) NDVI, Enhanced Vegetation Index (EVI) and Normalized Difference Water Index (NDWI) have been developed from this data (Anderson *et al.,* 2007) and these remote sensing methods use vegetation to represent drought conditions. Monitoring can thus be achieved by observing the spectral change of vegetation in the visible and near infrared region(Marshall *et al.*, 2004). Based on these two spectral channels the NDVI is the most common and not only maps the presence of vegetation on a pixel by pixel basis but also provides measures of the amount or condition of vegetation within a pixel (Wan *et al.*, 2004). Time series of these vegetation indices at global scale with high temporal frequency are freely available at present and these include MODIS (Moderate Resolution Imagery Spectro radiometer), SPOT (Satellite Pour l' Observation de la Terre) VEGETATION and AVHRR(Advanced Very High Resolution Radiometer (Rojas *et al.*, 2011).

Environmental remote sensing monitoring and modelling can provide a synergistic means of observing changes in thermodynamic balance during drought onset whilst providing reliable projections accounting for variations and correlation of water vapour and heat fluxes (Gao *et al.*, 2009). Different types of modelling systems have been developed over the years in order to use remote sensing inputs for surface flux estimation (Zhan *et al.*, 1996). In crop production, statistical, semi empirical and crop process can be used and more deterministic models such as the soil-vegetation –atmosphere transfer models (SVAT) simulate intermediary variables linked to

hydrological processes as well as give access to detailed description of soil and vegetation canopy processes that are not only limited to final variables such as evapotranspiration and net primary production. SVAT models may intrinsically provide a mean for interpolating fluxes between remote sensing data and within these models, it may be possible to implement procedures to assimilate data acquired by a large range of remote systems which differ in wavelength domains, acquisition time or geometry (Olioso *et al.*, 1999). Agronomists need to assess various variables within the soil–canopy system such as LAI, light interception photosynthetic active radiation (PAR)(Delécolle *et al.*, 1992) in forecasting crop yield more accurately. Applications such as crop production and crop growth simulations require more accurate estimation of LAI of crop canopies (Delécolle, *et al.*, 1992). Remote sensing and LAI of crop canopies can be linked based on the relationship between red and infrared reflectance with LAI. Thus a provision of crucial information on important crop state variables on a regional scale is enabled. Combing remote sensing information and crop growth models further provides direct link between state variables and remote sensed data as well as independence from time the remotely sensed data acquired. This is because crop growth models provide continuous estimates of growth overtime while remote sensing provides a multispectral assessment of instantaneous crop condition within a given area (Delécolle, *et al.*, 1992).

1.2. Research Problem.

Modelling is typically necessary to provide means for interpolating between infrequent remotely sensed observations. When using a model like Surface Energy Balance System (SEBS) in modelling land surface fluxes, several sensitivity analysis have indicated that the SEBS Land Use automatic routines products are very sensitive to the NDVI, fractional vegetation cover and LAI resulting in a deeper analysis on the validation of this approach being advised for any particular application (SEBS Help).

1.3. Justification

A model such as SEBS over simplify reality and thus implies that fractional cover and LAI have to be accurately modelled in order to reduce the uncertainty that arises from such a process. Fractional cover and leaf area index are variables not entirely independent from each other and care should be taken in separating them when being modelled because LAI may partially account for fractional cover (Carlson *et al.*, 1997) and thus a method will be formulated that investigates the retrieval of LAI and fractional cover based on the established relationship between the two parameters. It is also shown that viewing zenith angle in combination with amount of vegetation and vegetation structure is shown to have an effect on the magnitude of errors in retrieval methods and it is therefore useful to take angular effects into account when applying land surface parameters in models (Rasmussen *et al.*, 2010). The novelty in this study is to improve land surface parameter retrieval to produce a comprehensible model that is easily applicable in improving the estimation of LAI and fractional cover for use in SEBS for Barrax Agriculture Study Site.

1.4. Research Objectives

This research aims to evaluate the improvement of retrieval of land surface parameters as input in to the SEBS model as compared to using by-products from the automated SEBS routines.

1.5. Specific Objectives

1. To formulate algorithms that produce better estimates of land surface parameters LAI and Fractional cover in comparison to automated SEBS routines.
2. Assess the influence of a non random sampling strategy in LAI retrieval from image data.
3. Evaluate the correction of surface parameter estimation through the inclusion of a viewing angle for remote sensing data.

1.6. Research Questions

1. To what extent does the low geolocation accuracy impact the sampling strategy in trying to reduce the effect of uncertainty in LAI and Fractional cover estimation?
2. Which model gives an improved estimation of LAI from Aster data and high resolution Airborne Hyper Spectral (AHS) data?
3. Is there a significant improvement in model estimation due to the correction of image data by multiplying with the cosine of the viewing angle?

1.7. Hypothesis.

For all model predicting LAI and Fractional cover the following hypothesis was formulated:

Qn1: H_0 : There is no significant improvement in the agreement in leaf area index (RMSE, R^2) if data pairs between image and field observations are obtained by areal population statistics rather than single point sampling techniques in addressing the mentioned geolocation inaccuracy issues

H_a : There is a significant improvement agreement in leaf area index (RMSE, R^2) if data pairs between image and field observations are obtained by areal population statistics rather than single point sampling techniques in addressing the mentioned geolocation inaccuracy issues

Qn2: H_0 : The new algorithms do not give better LAI and Fractional cover estimates as compared to the SEBS routines

H_a : The new algorithms give better LAI and Fractional cover estimates as compared to the SEBS routines

Qn3: H_0 : There is no improvement in the model estimation after correction of the image data by multiplying with the cosine of the viewing angle

H_a : There is an improvement in the model estimation after correction of the image data by multiplying with the cosine of the viewing angle

2. LITERATURE REVIEW

2.1. Land Surface Parameters retrieval from satellite data

2.1.1. Leaf Area Index

Leaf Area Index (LAI) characterizes the canopy atmosphere boundary where most of the energy fluxes exchange occurs. LAI is a biophysical variable that is important in defining structural properties of a plant canopy. It is used to quantify the interception of light by the canopy and is viewed as a succession of absorbing layers of leaves each reducing radiation. LAI can be used to calibrate crop growth models and coupled vegetation and hydrological models. When it comes to estimating fractional cover in context of the big leaf model as it is done in the SEBS model, fractional cover of a homogenous vegetated land cover is defined as the percentage of soil which is covered by green vegetation, when looking vertically from the top (Jarvis, 1995). This is in respect to the size of vegetation that interacts with the atmosphere through evapotranspiration, absorbing radiation and storing energy and it is influenced by the area of leaves per area of ground.

Lhomme *et al.* (1988) states that LAI and Fractional cover are important parameters in processes such as land surface temperature retrieval where they contribute to what radiometers measuring the surface temperature of a crop canopy take into account in terms of radiative fluxes being emitted by all surfaces viewed by the instrument. Within a Far Thermal Infrared (FTIR) pixel with a vegetated portion, the temperature recorded by the radiometer is a function of the canopy temperature plus the temperature of the exposed soil. The vegetated portion can be translated into Leaf Area Index (LAI) which is greatly related to canopy process such as evapotranspiration as well as directly quantifying plant and canopy structure. LAI is useful in such a case in explaining the misrepresentation of aerodynamic temperature by radiative temperature as the degree of exposure of soil to radiation varies with different stages of growth implying also a variation of radiation emission by the soil measured at the sensor. Over regions characterized by fractional cover or row crops ,temperature measurements acquired by thermal infrared radiometers often reflect a mixture of soil and canopy temperatures (Friedl *et al.*, 1994). This depends on the view geometry of the sensor, the stability of the lower atmosphere and the temperature difference between the vegetation canopy and soil background. Accurate retrieval of surface temperature becomes complicated if measurements are made by sensors aboard satellite platforms far above the ground. Therefore in using remote sensing techniques to measure sensible heat fluxes over vegetated areas, differences have been observed, which results in thermal infrared temperatures not always representing aerodynamic temperatures. This aerodynamic temperature is needed in crop growth models which are useful in monitoring agricultural crops during the growing season. This is important in order to adjust the management (e.g. irrigation, fertilizers) and to provide information for obtaining yield predictions before harvest time as well as detect or forecast the threat of drought beforehand.

2.1.2. Gap Fraction theory

Gap fraction is measured in terms of the probability of light penetration and the amount of distribution and openings in the canopy relative to the chances that a light beam reaches the soil without contact with vegetation components. The theory of gap fraction therefore applies to the percentage or proportion of gaps for the whole hemispherical bottom up view of a canopy. It requires accurate modelling to predict light environment in the canopy, photosynthetic activity or canopy reflectance. Gap fraction is determined through the geometrical structure of the canopy, i e a data set describing location, orientation, size and shape of the vegetation components (Ross, 1981).

A comprehensive explanation of the canopy structure is quite an idealistic scheme because of the amount of Information required and therefore the structure is generally summarised by a few synthetic variables like the leaf area density and the leaf orientation distribution. The leaf area density, $l(h)$ at level h in the canopy is well-defined as the leaf area per unit volume of canopy. The leaf area index, L, at a level H in the canopy is related to the leaf area density through:

$$L = \int_0^H l(h)dh \tag{1}$$

The mean number of contacts $N(H,\theta_v,\varphi_v)$ between a light beam and a vegetation element at a given canopy level H in the direction for which the incident light beam penetrates inside the canopy (θ_v,φ_v) is given by:

$$N(H,\theta_v,\varphi_v) = \int_0^H G(h,\theta_v,\varphi_v)l(h)/\cos\theta_v dh \tag{2}$$

Where $G(h,\theta_v,\varphi_v)$ is the projection function, i.e. the mean projection of a unit foliage area at level h in direction for which the incident light beam enters inside the canopy (θ_v,φ_v). When the leaf area density and the projection function are thought to be independent of the level h in the canopy, Eq. 2 is simplified into Eq. 3:

$$N(L,\theta_v,\varphi_v) = G(\theta_v,\varphi_v)L/\cos\theta_v \tag{3}$$

The projection function is defined as follows:

$$\begin{cases} G(\theta_v,\varphi_v) = \dfrac{1}{2\pi}\displaystyle\int_0^{2\pi}\int_0^{\pi/2}|\cos\psi|g(\theta_l,\varphi_l)\sin\theta_l d\theta_l d\varphi_l & (4a) \\ \cos\psi = \cos\theta_v\cos\theta_l + \sin\theta_v\sin\theta_l\cos(\varphi_v-\varphi_l) & (4b) \end{cases}$$

Where $g(\theta_l,\varphi_l)$ is the probability density function that describes the leaf normal orientation distribution function (*i.e.* the fraction of leaf area with a normal within the solid angle $d\Omega_l$, in the direction Ω_l .This introduces the two normalization conditions given in Eq 5a and 5b:

$$\begin{cases} \frac{1}{2\pi}\int_0^{2\pi}\int_0^{\pi/2} g(\theta_l,\varphi_l)\sin\theta_l d\theta_l d\varphi_l = 1 & (5a) \\ \frac{1}{2\pi}\int_0^{2\pi}\int_0^{\pi/2} G(\theta_v,\varphi_v)\sin\theta_v d\theta_v d\varphi_v = \frac{1}{2} & (5b) \end{cases}$$

The definition varies according to author $g(\theta_l,\varphi_l)$ but may also be defined as the leaf angle distribution, *i.e.* the fraction of leaf area for which the angle between the vertical and the normal of the leaf is between θ_l and $(\theta_l + d\theta_1)$ together with the azimuth is between φ_l and $(\varphi_l + d\varphi_1)$ In this case, Eq 5a should be written as (Sinoquet and Andrieu, 1993):

$$\frac{1}{2\pi}\int_0^{2\pi}\int_0^{\pi/2} g(\theta_l,\varphi_l)d\theta_l d\varphi_l = 1 \quad (6)$$

The contact frequency is a very attractive quantity to indirectly estimate LAI because no assumptions on leaf spatial distribution, shape, and size are required. Unfortunately, the contact frequency is very difficult to measure in an illustrative way within canopies and thus the gap fraction is generally preferred. In the case of a random spatial distribution of infinitely small leaves, the gap fraction $P_o(\theta_v,\varphi_v)$ in (θ_v,φ_v) direction is related to the contact frequency by:

$$P_o = e^{-N(\theta_v,\varphi_v)} = e^{-G(\theta_v,\varphi_v)L/\cos(\theta_v)} \quad (7)$$

This is known as the Poisson model (Weiss *et al.*, 2004).

2.2. Viewing Angle Effects in Land Surface parameter retrieval

Physical features of an area have an influence on the radiance and this can effectively alter the angle between viewer, earth and sun. Therefore measurement of the emission of different cover types becomes influenced by the viewing angle of the sensor as different sections of the ground cover fraction of the crop will be visible at different viewing angles. The sensor can see only a single part of the plant depending on view angle , crop diameter plant distance and crop height(Vonder *et al.*, 2000). It is such that when a sensor moves from nadir to off-nadir viewing the sides of the canopy come into view and make the soil obscure resulting in an increased foliage area viewed by the sensor (Ranson *et al.*, 1985). Taking into account the multi angle measurement provides a distinctive way of implying surface information within the observed pixel(Chopping, 2008) and the prediction of plant geometry parameter such as height , diameter and crop coverage may be possible(Vonder, *et al.*, 2000). Differences have been observed when estimating LAI or fractional cover from remote sensing because the variability of viewing angle affects measurement at the sensor should be considered if uncertainties and the production of errors are possible due to a model's sensitivity to its input parameters. Therefore in some cases multi angular measurement may offer vividly canopy structure leaf properties soil moisture and radiation variables than mono-directional measurements(Chopping, 2008).

2.3. Modelling Systems of Land Surface Parameters

Remote sensing based methods for initializing, updating and validating land surface variables within these models still remains inadequate particularly the fact that virtually all of the dynamic components of land surfaces that influence and interact with the atmosphere are treated as prognostic variables (Friedl, 2002). The success of modelling techniques have been limited due to variables such as solar radiation, wind speed, air temperature and humidity, vegetation structure (leaf area index, height etc.) and properties, soil properties, moisture availability and viewing angle of the sensor. These variables have strong effects on the relationship between thermal radiance and partitioning of the energy and mass flux of the surface (Norman *et al.*, 1995) such as when solar radiation is incident on crop canopy, part of it is used in vaporization of water meaning that if less water is used more energy is left for canopy heating (Venus *et al.*, 2004) and this needs to be modelled appropriately.

2.3.1. Model Description

SEBS was developed with the goal of estimation of turbulent fluxes and surface evaporative fraction using satellite observed data. SEBS is an algorithm that calculates evapotranspiration by means of the surface balance index and computes fluxes from visible, near infrared and thermal radiances. The algorithm as described by Su (1999) has been implemented by Hans van der Kwast and Karssenberg in PC raster Python. It is a single source model with 3 module deriving energy balance terms, stability parameters and roughness length. Three sets of data inputs are required, (1) albedo, emissivity, temperature and NDVI, (2) meteorological data such as air temperature, humidity wind speed), (3) radiation data in the form of downward solar radiation and long wave radiation. Fractional cover and LAI are non-spatial outputs but the SEBS was adjusted such that it produced spatial maps from the calibrated algorithms.

2.3.2. Model Sensitivity to Input Parameters

SEBS estimates evaporative fraction and in order to improve model performance, sensitivity analysis has been carried out in order to determine the required precision of input parameters(Lin, 2006). Estimation of LAI and fractional cover as input parameters in modelling of evapotranspiration by SEBS hinges on their proper estimation to balance out the model's sensitivity. Accurate estimates by SEBS are important since the knowledge of evapotranspiration rates is an essential aspect for managers responsible for managing and planning for water resources primarily in arid & semi-arid regions where crop water demands are more than water received through rainfall. Irrigation from surface and/or groundwater resources is then required to meet the deficit. Accordingly knowledge of evapotranspiration rates is useful in understanding this water demand by plants and this is based on the fact that under normal conditions plants transpire and as water evaporates it cools the leaves but in periods where there is insufficient water, transpiration is minimal.

In SEBS fractional cover is a user defined product and for different purposes it uses different formulation of fractional cover. Therefore it is important to note the choice of formula and its calibration since it has a subsequent effect on evapotranspiration(Gibson *et al.*, 2011). According to Lin (2006) SEBS modelled evaporative fractions increased with increasing fractional cover that the SEBS evaporative fraction is more sensitive to high NDVI value areas. Van der Kwast *et al* (2009) in relation to sensible heat flux mentions that, although there is a lesser sensitivity of SEBS derived sensible heat flux to errors in surface aerodynamic parameters as compared to

surface temperature, the errors in the approximation of these parameters from remote sensing images using empirical relations can be larger and surpass the 50% limit of input accuracy for many land cover types.

3. STUDY AREA AND DATASETS

3.1. Study Area

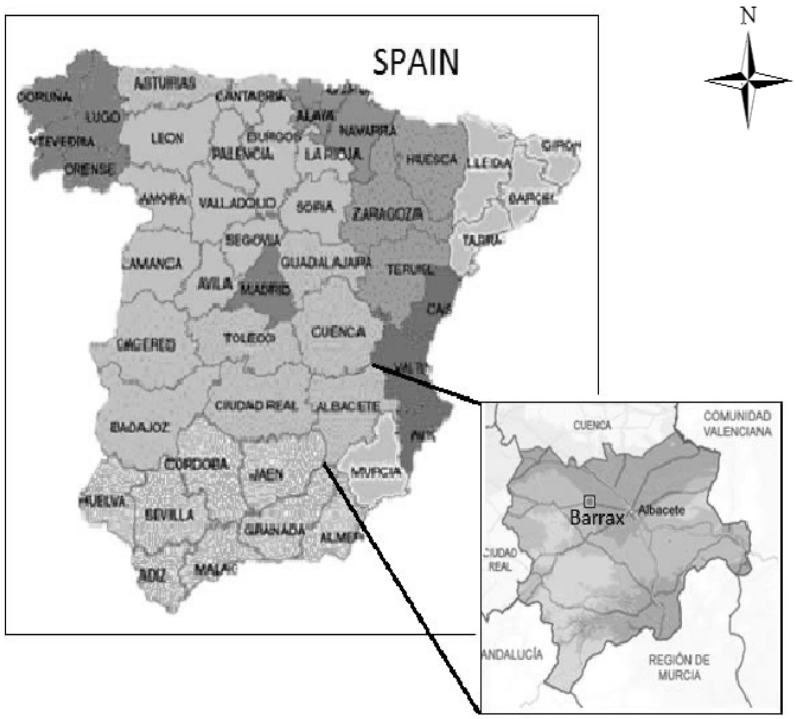

Source: Map of Spain[1] (left) and Barrax Study Site[2] (bottom right)

Figure 1: Location of Barrax Study Site

The study area (Figure 2) is the Barrax test site which is rectangular in form covering 50km², with coordinates related to Zone 30 Datum WGS 84 and corner coordinates as in Table 1. It is located in the region La Mancha a plateau 700m above sea level south of Spain. Climatic conditions are of high precipitation in spring & autumn and the minimum in summer and the annual rainfall averages 400mm. La Mancha has high thermal oscillations during all seasons and it is the driest area in Europe.

Table 1: Geographic coordinates of the study site.

Geographical corner coordinates		
Corner 1	575505.9523E	4323210.7146N
Corner 2	585226.6519E	4325555.7469N

[1] http://www.theodora.com/maps/
[2] http://www.vacances-location.net/vakantiehuizen/vakantiehuizen-barrax,albacete.thtml

Corner 3	575039.5028E	4325144.3194N
Corner 4	584760.2034E	4327489.3472N

Source: (Valencia, 2011)

The area is characterized by flat morphology and large uniform land-use units and consists of 65% dry land and 35% irrigated land with large pivot and other different agriculture units. The area has been used for agriculture.

3.2. Description of Data

3.2.1. Remote Sensing Data

Remote sensing plays a vital role in real time monitoring of agricultural conditions over a large area and thereby effectively supplementing the ground mechanisms (Krishna et al., 2009). Satellite data can be used in monitoring crop growth which yields required parameters for crop growth modelling on a real-time and area basis. The satellite images of different resolutions were used in the study. Advanced Space borne Thermal Emission and Reflection Radiometer (ASTER) is a sensor aboard one of NASA's Earth Observation System (EOS) satellite. It has a wide spectral range and higher spectral resolution of 0.52-11.65 microns with 14 bands. It also provides a multi spectral infrared data (8-12 microns window region globally). Aster images also have a high spatial resolution at 15m, 30, and 90m. One scene of Aster image acquired on 18th of July 2004 was applied in this study and this was Level 1B product of which the Aster channels were radiometrically calibrated and geometrically co-registered. A description of the Level 1B product is summarized in Table 2

Table 2: Description of ASTER spectral bands

Subsystem	Band number	Spectral range	Spatial Resolution
VNIR	1	0.52-0.60	15m
	2	0.63-0.69	
	3N	0.78-0.86	
	3B	0.78-0.86	
SWIR	4	1.600-1.70	30m
	5	2.145-2.185	
	6	2.185-2.225	
	7	2.235-2.285	
	8	2.295-2.365	
	9	2.360-2.430	
TIR	10	8.125-8.475	90m
	11	8.475-8.825	
	12	8.925-9.275	
	13	10.25-10.95	
	14	10.95-11.65	

The Airborne Hyper Spectral (AHS) data was collected from the INTA AHS system where an 80-band line scanner radiometer is installed in a CASA C-212 aircraft and integrated with GPS/INS POS-AV 410 FROM Applanix. The radiometer design is such that in the MIR and TIR ranges it has a high spectral resolution (30nm to 50nm) and the atmospheric windows (3-15microns and 8-15microns) are fully covered. Raw data was transformed to sensor radiance (level 1b) and later geo-located based on the processing of GPS/INS data synchronized with imagery at sensor radiance (level 1c). The AHS data was sampled to a 2m resolution providing very high resolution data for the study site. Image used in the study was of 18 July 2004 that was of a time close to the satellite overpass with the ASTER image SPARC Report (ESA, 2005).

Table 3: AHS spectral configuration

	PORT 1	**PORT 2A**	**PORT 2**	**PORT 3**	**PORT 4**
coverage(micrometres)	0.43 ->1.03	1.55 -> 1.75	2.0 -> 2.54	3.3 -> 5.4	8.2 -> 12.7
bandwidth (FWHM)	28 nm	200 nm	13 nm	30 nm	40-50 nm
$\lambda/\Delta\lambda$ (minimum)	16	8	150	110	160
nº of bands	20	1	42	7	10

The satellite data was pre-processed for PCRaster version for SEBS to generate variables fractional cover, NDVI and LAI.

3.2.2. Ground Data

In–situ measurements were part of the SPARC-EAGLE campaign carried out from 12-21 July 2004 at Barrax agricultural study site in Spain. Ground Observations of LAI were obtained from an indirect LAI retrieval method using LAI-LI COR 2000 instrument. One ambient light measurement was obtained with the sensor extended at arm's length, upwards over the top of the canopy and then 8 below canopy readings with this pattern being repeated per spot (ESA, 2005). The measurements were taken in fields of alfalfa *(Medicago sativa L.),* corn *(Zea mays L.),* garlic *(Allium sativum L.),* onion *(Allium cepa L.),* potato *(Solanum tuberosum L.)* and sugar beet *(BetaVulgaris L.)* as shown by Fig 2.

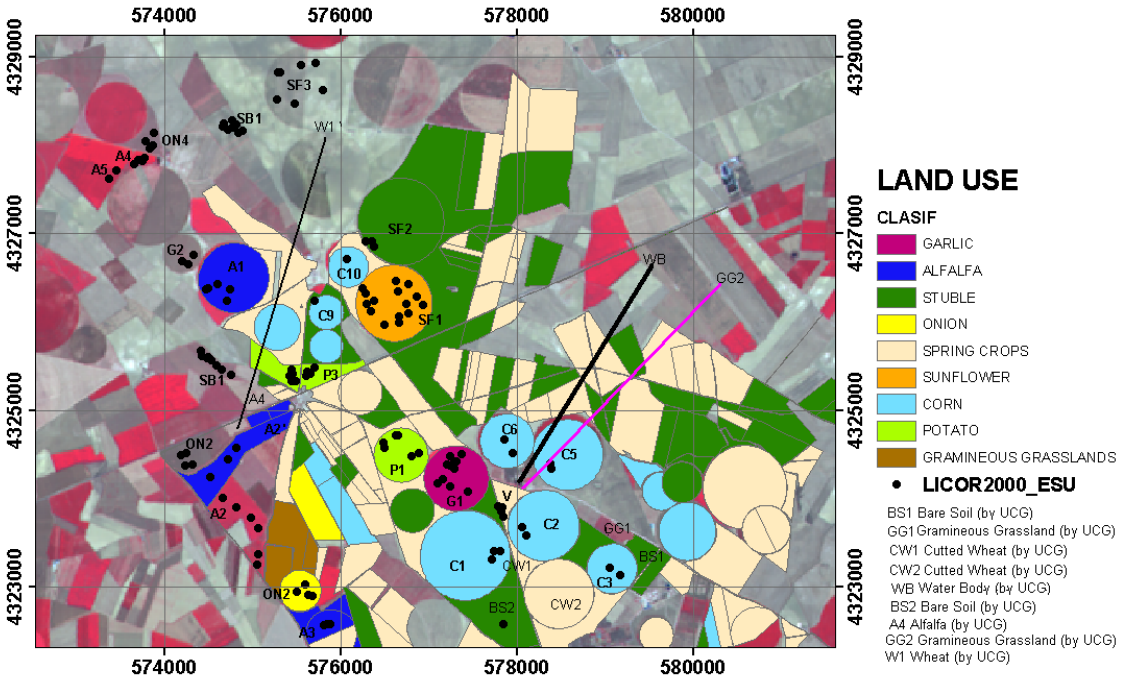

Figure 2: Land use map showing locations of LICOR LAI measurements

Furthermore Fig3 shows LAI measurements from hemispherical photographs that were preprocessed with WinPhot and used in the analysis of ground observed fractional cover.

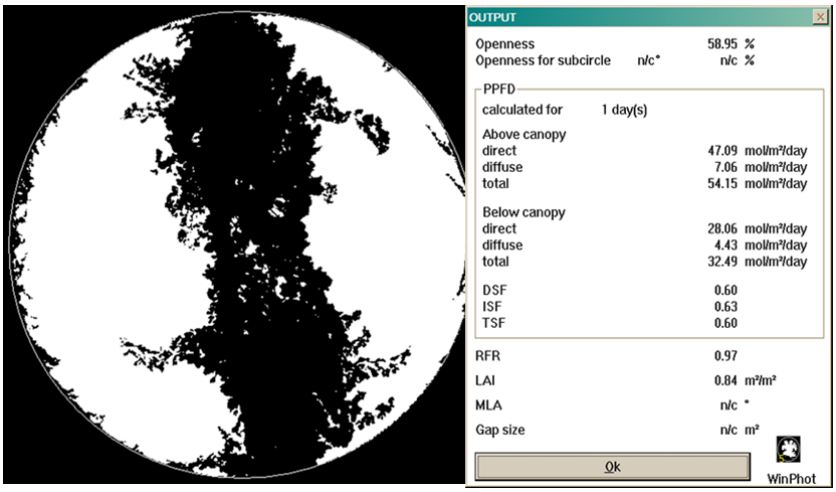

Figure 3: Hemispherical photographs showing calculations using WINPhot software.

4. METHODOLOGY

4.1. Sampling Strategy

Positional accuracy relates to the accuracy of a point on the imagery with reference to its physical location on the ground and thus for any comparison it is important that the same location be located both on the image and on the ground (Congalton, 2005). Generally geo-referencing images and using global positioning systems (GPS), locational errors can be reduced. However there is still uncertainty about whether the field location is tied to a single pixel coordinate (Forsythe, 2006) and for this reason it was necessary to estimate a potential locational error in pixel units and adjust accordingly in relation to the ground sample unit size. Sampling strategy is therefore important in order to be able to provide reliable estimates of land surface parameters in crop growth simulations. In this study to get representative measurements of LAI from satellite data, coordinates of the ground measurements were converted to point map and the generated point map was overlaid on the images to get representative LAI observations that coincided with ground measurements. Some points were off their actual position, that is to say a point representing a sample in the maize field was then located on the road beside the field when the point where overlaid on the image and therefore a qualitative sampling method had to be devised. The uncertainty causing the shift in the points was attributed to GPS error sources such as noise, bias, blunders (mistakes due to computer or human errors) of which their combined magnitude does indeed affect the accuracy of the positioning result.

Table 4: Cumulative error of a standard Garmin GPS

Error	**Value**
Ionosphere	4.0 meters
Clock	2.1 meters
Ephemeris	2.1 meters
Troposphere	0.7 meters
Receiver	0.5 meters
Multipath	1.0 meter
Total	**10.4 meters**

Based on the type of GPS used a summary (Table 2) of the potential cumulative error was created and it was used to generate buffers around the points. Purposive sampling was executed through a rank order method to hand pick LAI values. The design was such that for a cluster of sample points, a rank order was created based on the ground observation and the area was stratified according to crop type and individual field location. The point observation from one stratum with the highest ground observed LAI value was ranked as 1 and the next highest was ranked as 2 and so on.

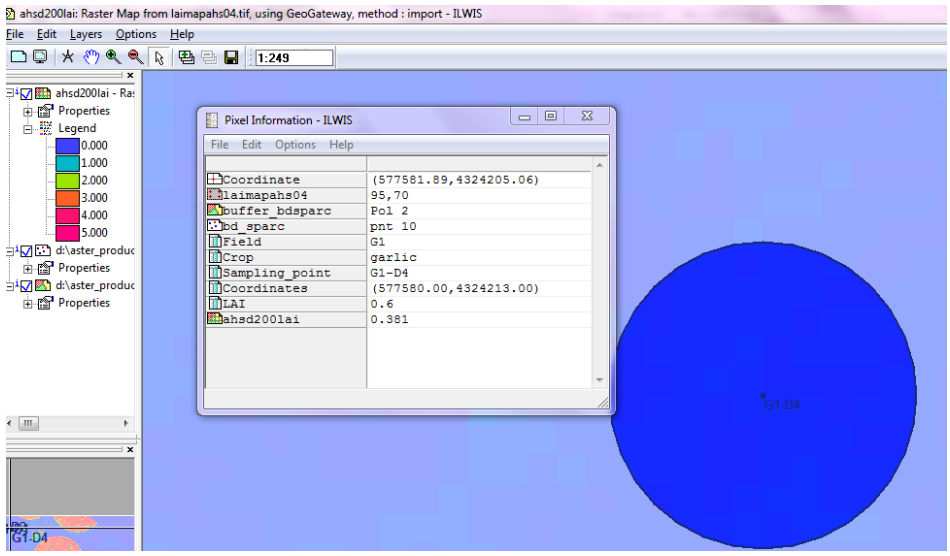

Figure 4: Sampling on LAI values from the image.

4.2. LAI Retrieval

NDVI and LAI maps were generated based on automatic routines in PC Raster and imported into ILWIS. This was used together with an Aster LAI and NDVI product to test the suitability of a hand picking technique as part of a sampling strategy as well as compare the degree of estimation of LAI from automated SEBS and the exponential law based method (Bsaibes et al., 2009).Two LAI retrieval methods were based on the following equations;

Leaf Area Index (LAI) is internally calculated by SEBS as:

$$LAI = (NDVI \cdot (1 + NDVI)/(1 - NDVI))^{0.5} \quad (8)$$

1. **The exponential law based method** (Bsaibes, *et al.*, 2009) derived from the widely used works of (Asrar *et al.*, 1985; Baret *et al.*, 1991; Wilson *et al.*, 2007) calculate LAI as:

$$LAI = -\left(\frac{1}{K_{LAI}}\right) \cdot \ln\left(\frac{NDVI - NDVI_{\infty}}{NDVI_s - NDVI_{\infty}}\right) \quad (9)$$

$NDVI_s$ Is the bare soil NDVI value, $NDVI_{\infty}$ is the asymptotic value of NDVI when LAI tends towards the maximum value and K_{LAI} is an extinction coefficient. Parameters $NDVI_{\infty}$, K_{LAI} and $NDVI_s$ were adjusted using an optimization approach to minimise the Root Mean Square Error (RMSE).

Whilst taking into account the variability of the viewing angle Equation 9 was modified by multiplying with the cosine of the viewing angle such that the equation translates to;

$$LAI = \left(-\left(\frac{1}{K_{LAI}}\right) \cdot \ln\left(\frac{NDVI - NDVI_{\infty}}{NDVI_s - NDVI_{\infty}}\right)\right) \cdot \cos\theta \quad (10)$$

4.3. Agronomic Parameterization of Fractional cover

The crop coverage (CFLEAF) is described using the relationship between fractional cover and LAI (Bouman et al., 1992) as;

$$CFLEAF = 1 - \exp(-ke \cdot LAI) \tag{11}$$

Where ke is the coefficient of extinction and LAI is the leaf area index.

Light interception (ke) is a useful parameter in the calculation of crop coverage and its measurements are usually made close to solar noon when the solar angle is close to 0°. At this angle factors like row orientation and canopy height impact have a less contributory impact on what is measured. In this study the light extinction coefficient (ke) for only sites(corn and vine yard locations) where hemispherical photographs were available was calculated from transmitted photosynthetic active radiation (TPAR) and incoming photosynthetic radiation (IPAR) data by;

$$\frac{TPAR}{IPAR} = \exp \cdot (-ke \cdot LAI) \tag{12}$$

Or

$$k = -\frac{\ln\left(\frac{TPAR}{IPAR}\right)}{LAI} \tag{13}$$

4.4. Physical Parameterization of Fractional cover

The heterogeneous nature of land surfaces results in mixed pixels of anisothermal objects existing in far thermal infrared imagery at relatively coarse spatial resolution (Liu *et al.*, 2008). Thus variation in the reflectivity of vegetation materials may result in the misclassification of data from aircrafts and satellites if angular effects are not considered (Rao *et al.*, 1979; Shibayama *et al.*, 1985). However crops have a different leaf orientation and LAI when viewed at a low oblique angle (<45°) than when viewed vertically (Rao, *et al.*, 1979) such that it is necessary to explicitly bring out the influence of the viewing zenith angle on the measurement by the sensor. Anthoni *et al* (2000) suggest that there is an improvement in the estimation of upwelling radiation at the radiometer location over orthogonal cover fraction estimate and express average vegetation fraction ($f_{vegetation}$) as a function of viewing angle according to (Norman, *et al.*, 1995) as;

$$f_{vegetation} = 1 - \exp\left(\frac{-ke \cdot LAI}{\cos\theta_v}\right) \tag{14}$$

And the fraction of ground exposed within the canopy is represented as

$$f_{soil} = 1 - f_{vegetation} \tag{15}$$

This is because as a satellite scans over the earth, it encounters different terrains within its footprint which impacts the geometry of the angle, between viewer, earth and the sun for each pixel.

In this case however following the Poisson model and assuming the G- function for a spherical distribution to be 0.5 in place of ke Eq.14 becomes:

$$f_{vegetation} = 1 - \exp\left(\frac{-0.5 \cdot LAI}{\cos\theta_v}\right) \quad (16)$$

To address the uncertainty in obtaining data pairs between image and field location, the median and 95th percentiles were extracted from the areal population statistics of pixels lying within the uncertainty zone around the reported GPS-location as is exemplified in Fig. 4.

4.4.1. Statistical Analysis

To check whether there is an improvement in the calculations by the equations, the Bias, Root Mean Square Error (RMSE) were together to diagnose the variation in the errors in each equation. The Bias checks whether the models were overestimating or underestimating and was calculated using the following equation:

$$Bias = \frac{1}{n}\sum_{i=1}^{n}(f_i - y_i) \quad (17)$$

Where f_i are the observed values and y_i is the predicted values

RMSE is the average magnitude of absolute errors and is denoted

$$\sqrt{\frac{\sum(f_i - y_i)^2}{n}} \quad (18)$$

Where f_i are the observed values and y_i is the predicted values

5. RESULTS AND DISCUSSION

5.1. Sampling Strategy

Although stratification was based on crop type, sampled values were influenced by field location and management practices such that a point observation would be ranked low in terms of LAI ground observation but the values within the entire buffer for NDVI for that particular point would be higher than another sample point with a higher LAI ground observed value than it.

5.2. LAI Retrieval

In order to ascertain the possibility of estimating LAI using the empirical relationship between LAI and vegetation indices (NDVI), ground based measurements were analysed as a function of NVDI (Figure 5). Results showed that NDVI values saturated at an LAI of 3.5 for the fields in the study site. This is in line with the findings of Asner *et al* (2003) that at low LAI values spectral vegetation indices such as NDVI are sensitive to LAI but the relationship becomes weak and nonlinear as the values rise above 3 (Baret & Guyot, 1991).

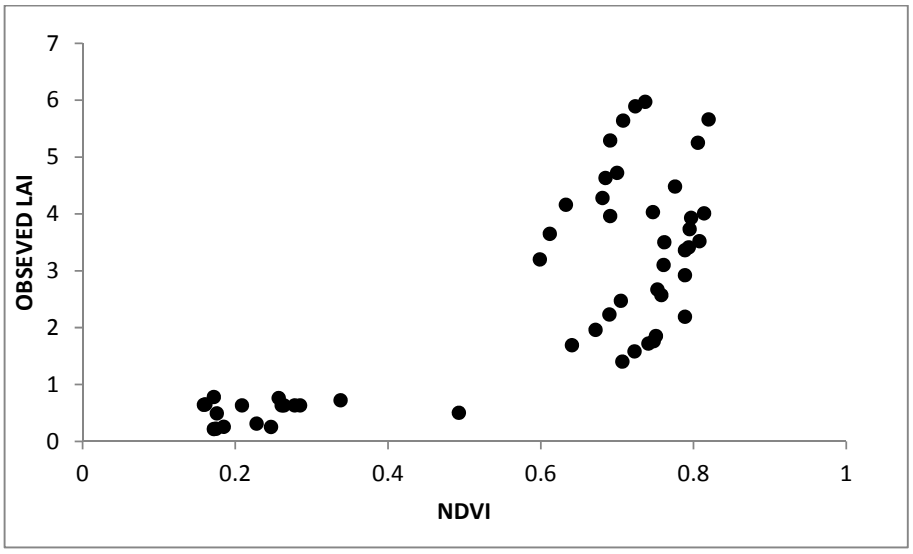

Figure 5: Relationship between Observed LAI and NDVI

For the inverted modified version of the Beer's law to measure LAI a site if unique values for the parameters were set and these are represented in Table 2 where the set of unique parameters that were established by least squares optimisation for both the AHS and the ASTER data.

Table 5: Adjusted parameters for the Exponential Model

	K_{LAI}	$NDVI_o$	$NVDI_s$

AHS	0.86	0.83	$1.08 \cdot 10^{-10}$
Aster	0.61	0.81	$1.08 \cdot 10^{-19}$

In comparison to the work of Bsaibes *et al.* (2009) the values are comparatively low for the ASTER data with a K_{LAI} of 0.61 as compared to that of their study of 0.71 and the $NDVI_{\infty}$ of 0.81 of the current study against that of 0.89 . For the AHS data, only the K_{LAI} differed and it was much higher in comparison. The differences observed may be attributed to the differences in crop cover type.

After the calibration of the exponential model, a comparison was made between SEBS automated routines and the calibrated model. Figure (6) show the relationship between observed and Estimated LAI retrieval of the two methods on the AHS data and Figure (7) show the relationships between LAI estimated by the two methods and the observed LAI measurements on the Aster data. For the AHS data the exponential law model over predicted LAI as compare to SEBS algorithm with Bias of 1.006 for the exponential model and 0.6004 for the AHS. This was quite contrary to the ASTER data that predicted LAI better than the exponential law model with a Bias of 0.514 and 0.968 for the exponential law and SEBS respectively.

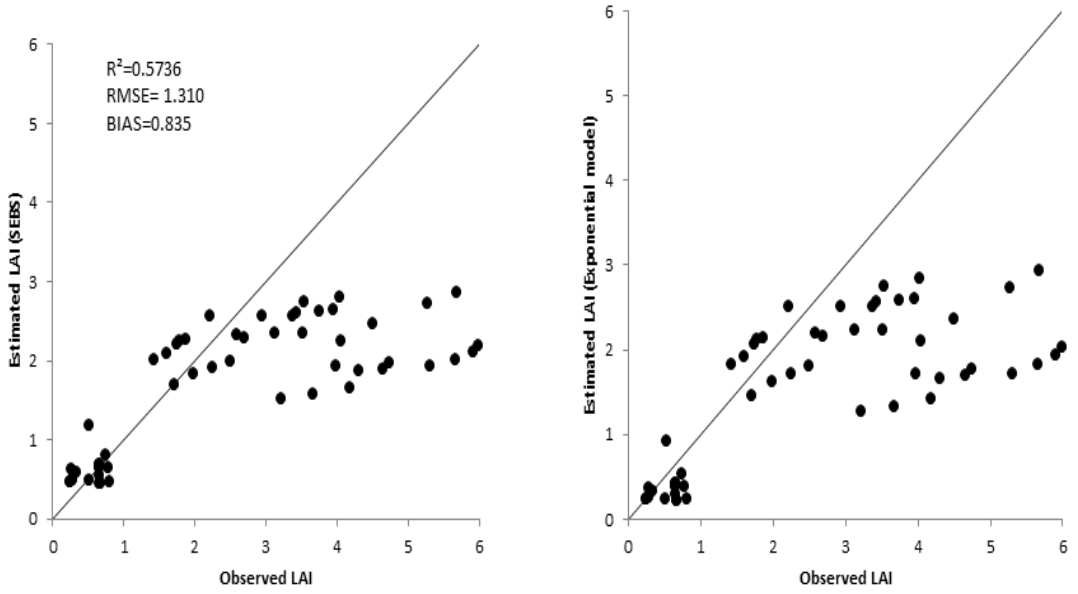

Figure 6: The relationship between observed and Estimated LAI retrieval methods on the AHS data.

In comparison to the ground observation, both models under predicted LAI and thus exhibited a relatively weak predicting power on both the ASTER and the AHS data. The Aster data however showed a better R^2 0.6249 and 0.6004 for the SEBS algorithm and the exponential model respectively with the scatter produced on the Aster data by the exponential model representing results more closely to the ground data.

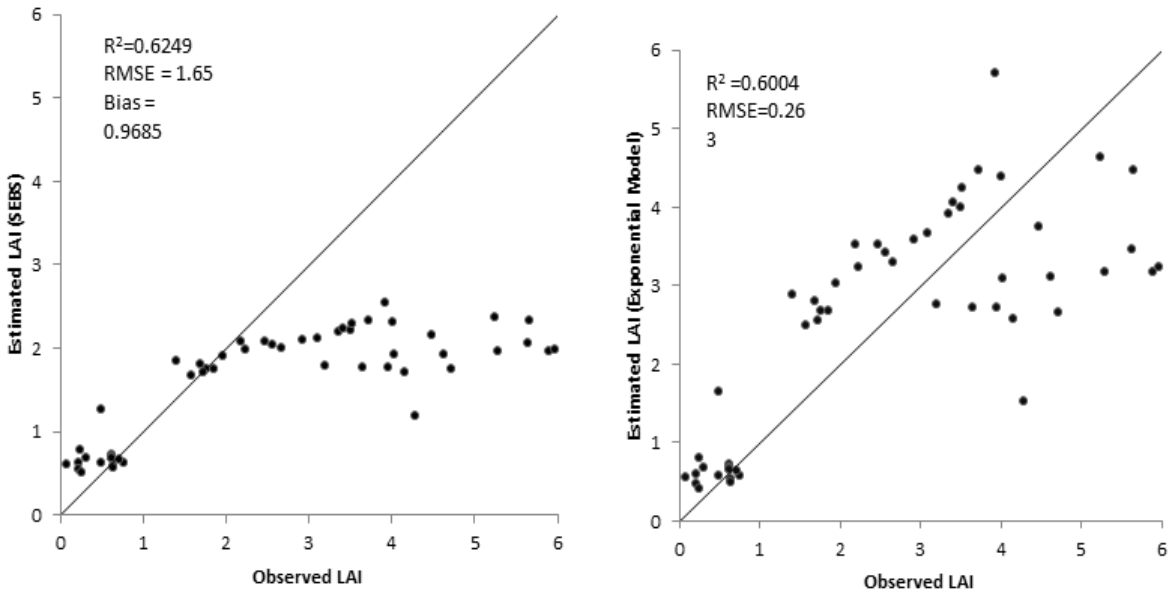

Figure 7: The relationship between observed and estimated LAI of the two methods on the ASTER data.

The much weaker performance of the SEBS algorithm in this study may be attributed to the fact that there the relationship between LAI and the NDVI is only strong at low NDVI values and according to Carlson and Ripley (1997) at low LAI values that were dominant in the study of less than 3, vegetation indices such as NDVI tend to be more closely related to fractional cover than to LAI of clumped vegetation. Also according to Asrar *et al.* (1985) LAI has a better correlation with NDVI for single plant species grown under uniform conditions but not for mixed canopies ,which often occurs in remote sensing studies where a single pixel can contain several landscape units a condition which is applicable to our study site which has different cropping units adjacent to each other.

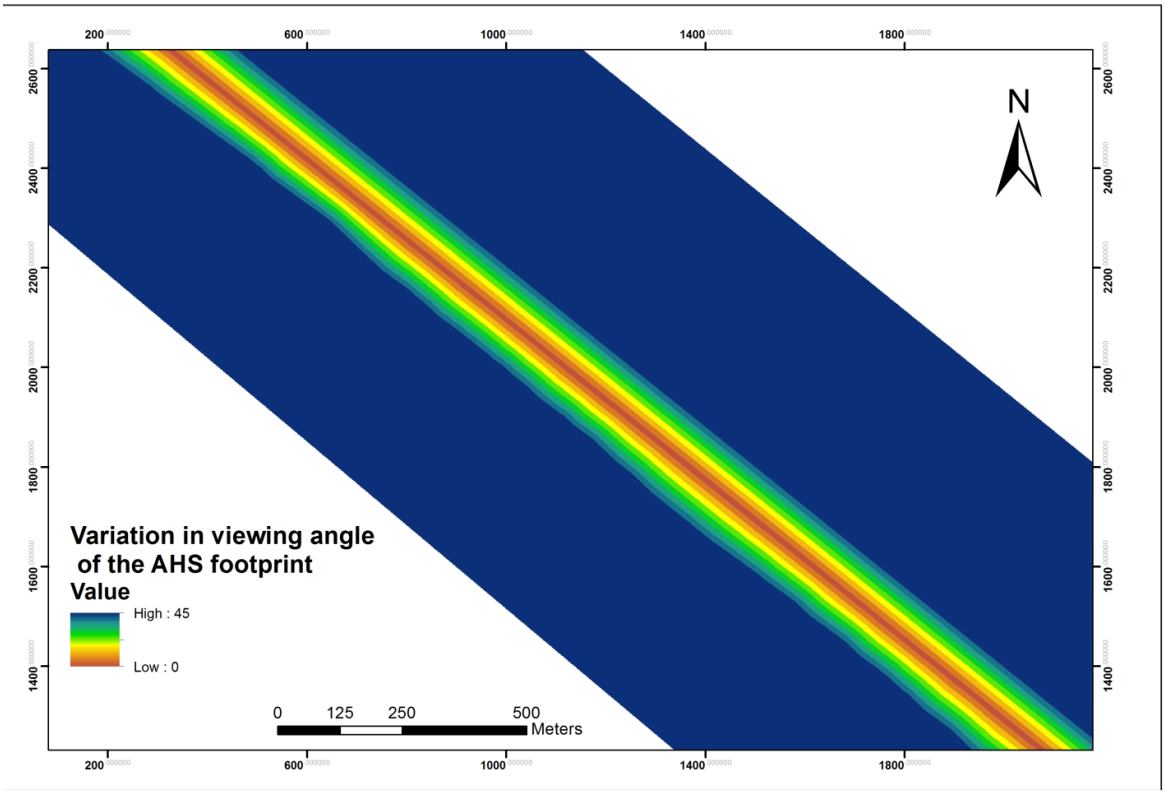

Figure 8: Variation in viewing angle of the AHS footprint

A map(Fig:8) was generated in order to extract the viewing zenith angle of the AHS swath and sample points of both LAI and fractional cover were over laid on the image. This allowed the exponential model to be further adjusted in order to investigate the incorporation of the viewing zenith angle to aid in its retrieval of LAI and fractional cover retrieval. The estimation of LAI and fractional cover was greatly affected by the viewing angle. With Equation (14) dividing with the viewing angle served to increase the estimation of fractional cover. The two equations were then compared model 1 (Equation 9) and model 2 (Equation10) for LAI estimation to see if the correction by multiplying with the cosine of the viewing angle improved the estimation of LAI. As estimators, the median and percentile of the models were obtained by the least squares method and Table 6 shows the resultant coefficients. The use of the median values resulted in an improved estimation of LAI and this is shown by the Root Mean Square Error (RMSE) of the model with the median as the estimator being lower (model 2: RMSE= 1.624131, model 1: RMSE=0.611678) than the percentile (model1: RMSE=1.622595, model 2: 1.521922).

Table 6: Adjusted parameters between the models

	model 1		model 2	
	95th-percentile	median	95th-percentile	median
NDVI∞	0.9	0.894358	0.9	0.9
NDVIs	1E-10	1E-10	1E-10	1E-10
KLAI	0.670174	0.6	0.611678	0.604497
RMSE	1.622595	0.611678	1.521922	1.624131

The results (Fig 9) show that the median estimation using model 3 had the lowest coefficients for all parameter and was the best predictor for LAI.

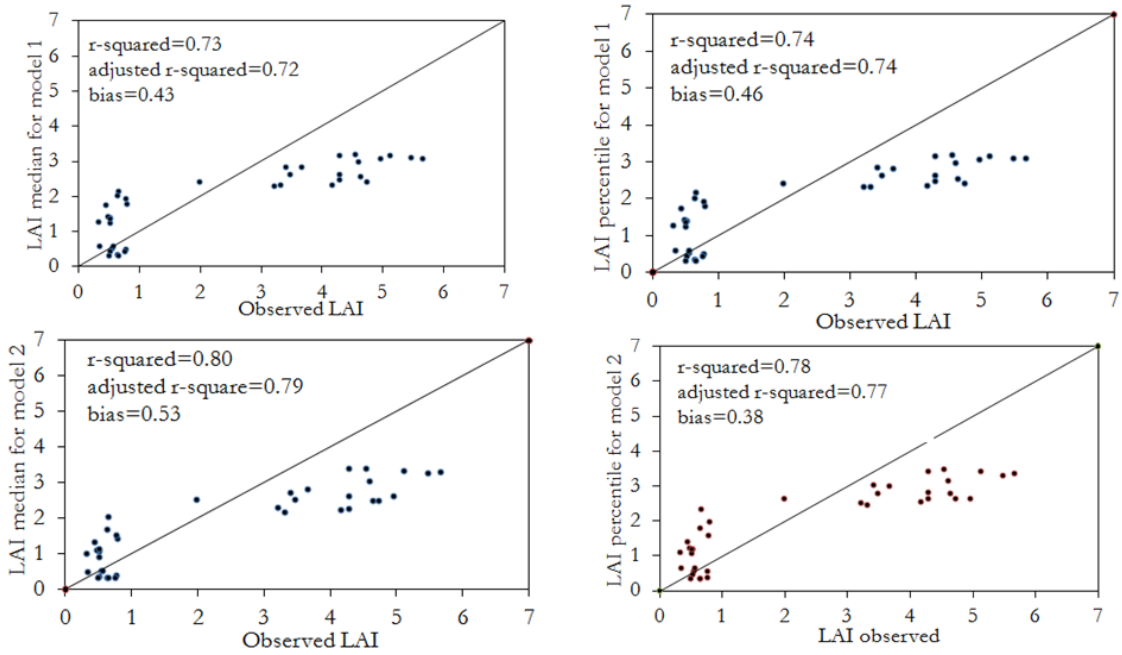

Figure 9: Comparison between LAI estimation by the two models each using the median and the percentile values respectively

All models were statistically significant, with all the P-values less than 0.05. Although all models were statistical significance model quality also had to be assessed. LAI model 2 Median produced a high R^2 on the validation points. Model 3-median was the best choice because the adjusted R^2

for the training dataset explained 80.3% of the variability in the response variable and it showed that the model fitted well to the observed values and only looking at the simple R^2 is biased upwards since it exaggerates the goodness of fit in a model with more than one variable. The model was overally highly significant (P-value = 1.9 x E-9 <0.05). The model predicted well on the validation data set (79.3%) meaning that there was little disagreement between the observed and the predicted values. This is important as it implies less error in predictions. Consequently the correction of the NDVI values by multiplying with the cosine of the viewing angle enabled better prediction of LAI as compared to assuming the conditions are at nadir when implementing these routines.

5.3. Parametirization of Fractional Cover

Fractional cover is also an important parameter soil-vegetation-atmosphere transfer models and surface energy balance models. The agronomic definition take into account assumes that the measurement is at nadir. Remote sensing estimation of fractional cover using the nadir assumption results in a non-representative estimation of fractional cover if the measurement is recorded at a particular angle. Due to the unavailability of sufficient data only a 19 points were used in this part of the study. These were used on Poisson model derivative for fractional cover estimation to compare with the agronomic physical parameterization of fractional cover.

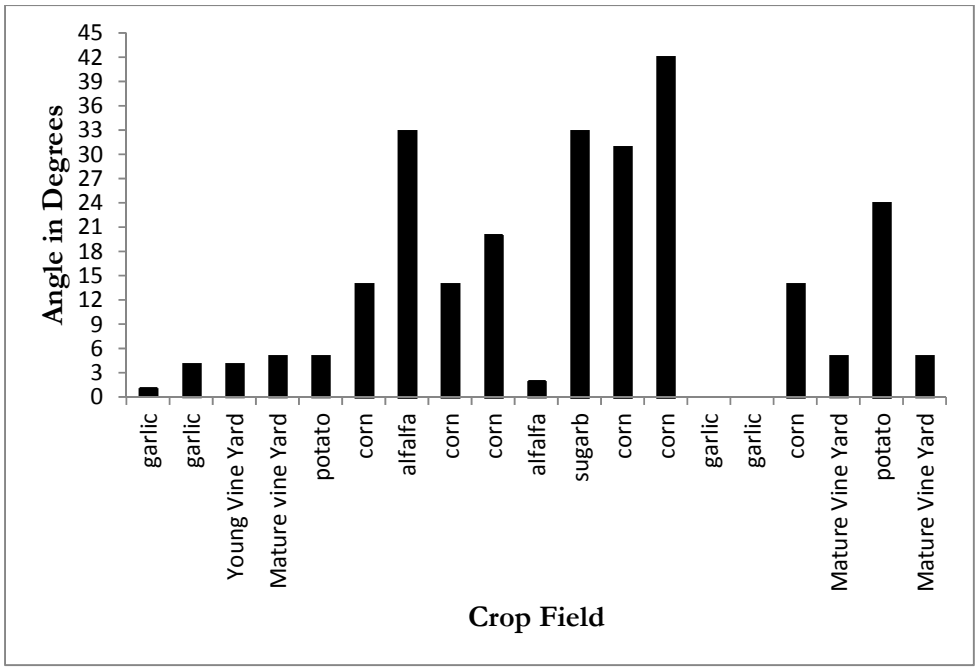

Figure 10: Variation in AHS viewing angle as per crop type

Figure 11 compares this phenomenon of the influence of correcting for the viewing zenith angle when using remote sensing data based on the viewing angle of 19 different crop samples with values shown in Fig 10:

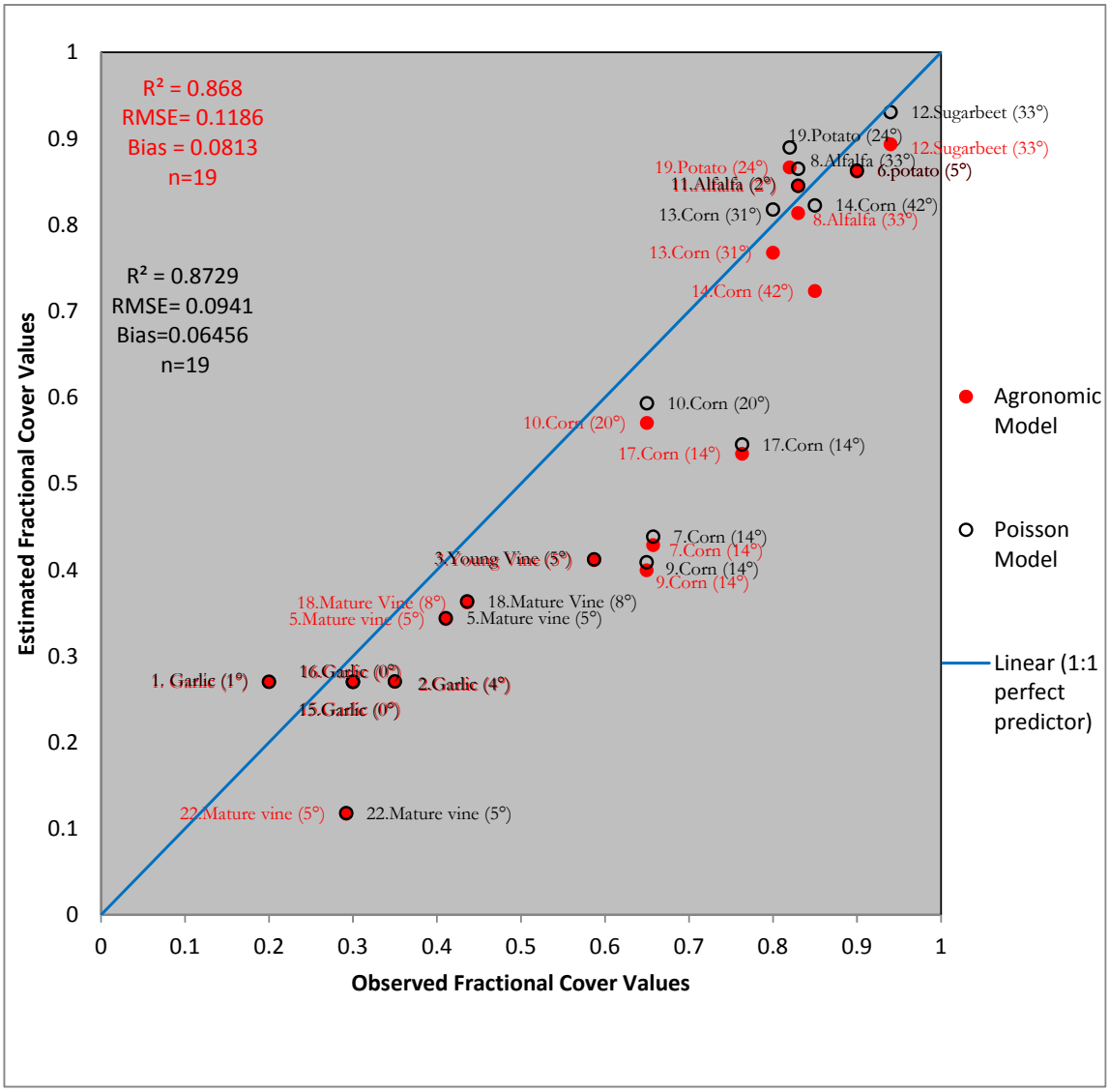

Figure 11: Comparison between Poisson model derivative and the agronomic model estimating fractional cover at different angles in relation to the perfect predictor.

Results show that at low viewing angle there is a negligible difference in the estimation of fractional cover by both models as shown by crops viewed at an angle between 0° and 8° (garlic and vine). As the angle increases marked differences in the positions of the points (Corn 14°) can be observed and this signifies that as the viewing angle increases, it impacts the predicting strength of the Poisson model. Multiplying with viewing angles at higher viewing angles served to increase the fractional cover and bring the value closer to the one to one line signifying that the values predicted by the Poisson model became closer to the expected values. However some

crops behaved differently, for example point 8 (Alfa Alfa 33°) in which case the fractional cover was either underestimated by the agronomic definition or over estimated by the Poisson model.

Leaf angle distribution and crop cycle of the crops played a role in the effect of the viewing angle of the sensor in fractional cover estimation. Planophiles which have a propensity to close their foliar canopies and equally shade lower leaves of crop canopy and from a nadir perspective the viewer can only see the effect of the canopy closure and yet at an angle the lower leaves can be observed and more representative fractional cover estimation can be obtained. This is shown in Fig. 11 by (point 6) where viewing a potato field at angle of 5° shows little difference between the models' prediction whereas at an angle of 20° (Point 19) an increase in fractional cover estimation is observed. Heliotrophic plants which reorient their leaves throughout the day to maximize exposure to the sun such as Alfa Alfa *(Medicago sativa L.)* and sunflower tend to be challenging and are difficult to estimate by incorporating the viewing zenith angle of sensor. Corn on the other hand although it exhibits asymmetrical leaf angle distribution, the change is not within one day as with heliotrophiles but the change is over time. This therefore means that the crop cycle of the corn plant will play a major role as it shifts from an erectophile distribution at an early stage of growth and as it fans out as it matures. Erectophile such as garlic are not drastically affected by the viewing angle and the fractional cover estimated was approximately the same for both models (points 1, 2, 15 and 16). The vine yard has a plagiophile distribution and remained the same as well since the field was measured at low angles.

Statistically results show a more pronounced difference in the models' estimation can be observed at higher values of the viewing angle. The difference is based on the R^2 (0.87) and RSME (0.09) of the Poisson model that showed the model performed better when multiplied by the cosine of the viewing zenith angle compared to the Agronomic model. This may be attributed to that in implementing the agronomic definition a bias is introduced if the viewing zenith angle is not accounted for when using remote sensing data. In this case this shown by the bias error calculated for the Agronomic being further from zero (0.0813) as compared to the Poisson model (0.06456). Overall the implication of this study is that when using a model like SEBS which is sensitive to fractional cover as input parameter, improper estimation will result in errors being introduced and subsequently propagated throughout the analysis. Gibson et al (2011) revealed that the sensitivity of SEBS to input parameters produced errors, if for example ill-defined NDVI limits were used in fractional cover retrieval. This error would subsequently be propagated further to soil and sensible heat flux up to evapotranspiration estimation.

6. CONCLUSION AND RECOMMENDATION

This chapter will serve to the research formulated in this study and this will be followed by limitations of the study and finally recommendations.

6.1. Conclusions

1. To what extent does the low geolocation accuracy impact the sampling strategy in trying to reduce the effect of uncertainty in LAI and Fractional cover estimation?

In the presence of a positional uncertainty, sampling procedure is of great importance such that the final output is not greatly affected by the uncertainty and error, potentially arising from the source of the data or through processing errors. Although acquisition of LAI is rather tedious and intensive is should nonetheless be as representative as possible, and thus there was a need for a robust estimator. The median produces a better RMSE in the event that the data has a high degree of uncertainty and the median proved to be a quick and useful parameter in counter acting the positional accuracy of the data. The low geolocation accuracy resulted in a non-random sampling technique centred on stratification based on crop type and field location and hand picking values. Though it served to provide some representation, it also aided in the propagation of errors in the analysis as is shown by the courser resolution aster image providing better results than the finer resolution AHS data.

2. Which model gives an improved estimation of LAI from Aster data and high resolution Airborne Hyper Spectral (AHS) data?

The issue of spatial heterogeneity and coarseness of data had an influence in the execution of the study. The exponential model produced the better results overally and especially when implemented on the resampled Aster data as compared to the AHS data which initially had the finest resolution of 15m. This marked difference between the ASTER and AHS results (although both images were finally sampled in the same resolution) could be attributed to errors that were accumulated in the processing of the images and also from the fact that non random sampling technique was used to hand pick the values on the image.

3. Is there a significant improvement in model estimation due to the correction of image data by multiplying with the cosine of the viewing angle?

LAI and fractional cover needed be modelled accurately as they are important components in land surface fluxes which serve to aid in understanding agriculture drought based on the knowledge of how much water a crop requires. Adjusting by multiplying with the cosine of the viewing angle served to improve the estimation of the Poisson model showing that indeed the variability in the angle at which the measurement of the surface parameters is done impacts the reading at the sensor and needs to be adjusted to represent reality. Canopy structure and characteristic will also determine will also affect the level to which this adjustment behaves

6.2. Limitations of this research.

During the course of this study, several challenges were encountered. The major drawback in carrying out this study was the quality of the data used. For the LAI measurements of ground observations there was not enough metadata available such that a lot of time was invested in trying to improve the positional accuracy of the measurements on the satellite images. Very few hemispherical photographs were available as another indirect method to measure LAI that were really useful for the study in order to investigate the retrieval of the light extinction coefficient (ke) for rowed crops. A consistent record of the data was also not available for the DOY of interest for all crops.

6.3. Recommendations

There needs to be a more detail study in the error propagation due to positional inaccuracy.
A much detailed statistical analysis is needed to compare various methods to minimize errors the estimation of parameters if the data is corrupted.
Further study into the validation of the degree to which the sensitivity of SEBS to fractional cover and LAI will be affected by this correction method needs a much deeper analysis.

LIST OF REFERENCES

Anderson, L. O., Malhi, Y., Aragao, L. E. O., & Saatchi, S. (2007, 23-28 July 2007). *Spatial patterns of the canopy stress during 2005 drought in Amazonia.* Paper presented at the Geoscience and Remote Sensing Symposium, 2007. IGARSS 2007. IEEE International.

Anthoni, P. M., Law, B. E., Unsworth, M. H., & Vong, R. J. (2000). Variation of net radiation over heterogeneous surfaces: measurements and simulation in a juniper–sagebrush ecosystem. *Agricultural and Forest Meteorology, 102*(4), 275-286. doi: 10.1016/s0168-1923(00)00104-0

Asner, G. P., Scurlock, J. M. O., & A. Hicke, J. (2003). Global synthesis of leaf area index observations: implications for ecological and remote sensing studies. *Global Ecology and Biogeography, 12*(3), 191-205. doi: 10.1046/j.1466-822X.2003.00026.x

Asrar, G., Kanemasu, E. T., & Yoshida, M. (1985). Estimates of leaf area index from spectral reflectance of wheat under different cultural practices and solar angle. *Remote Sensing of Environment, 17*(1), 1-11. doi: 10.1016/0034-4257(85)90108-7

Baret, F., & Guyot, G. (1991). Potentials and limits of vegetation indices for LAI and APAR assessment. *Remote Sensing of Environment, 35*(2–3), 161-173. doi: 10.1016/0034-4257(91)90009-u

Bouman, B. A. M., van Kasterend, H. W. J., & Uenk, D. (1992). Standard relations to estimate ground cover and LAI of agricultural crops from reflectance measurements. *Eur. J. Agron., 1*(4), 249-262. doi: citeulike-article-id:2472653

Bsaibes, A., Courault, D., Baret, F., Weiss, M., Olioso, A., Jacob, F., . . . Kzemipour, F. (2009). Albedo and LAI estimates from FORMOSAT-2 data for crop monitoring. *Remote Sensing of Environment, 113*(4), 716-729. doi: 10.1016/j.rse.2008.11.014

Campbell, G. S. (1986). Extinction coefficients for radiation in plant canopies calculated using an ellipsoidal inclination angle distribution. *Agricultural and Forest Meteorology, 36*(4), 317-321. doi: 10.1016/0168-1923(86)90010-9

Carlson, T. N., & Ripley, D. A. (1997). On the relation between NDVI, fractional vegetation cover, and leaf area index. *Remote Sensing of Environment, 62*(3), 241-252. doi: 10.1016/s0034-4257(97)00104-1

Chopping, M. J. (2008). Terrestrial Applications of Multiangle Remote Sensing

Advances in Land Remote Sensing. In S. Liang (Ed.), (pp. 95-144): Springer Netherlands.

Congalton, R. G. (2005). Thematic and Positional Accuracy Assess- ment of Digital Remotely Sensed Data. *Symposium A Quarterly Journal In Modern Foreign Literatures*, 149-154.

Delécolle, R., Maas, S. J., Guérif, M., & Baret, F. (1992). Remote sensing and crop production models: present trends. *ISPRS Journal of Photogrammetry and Remote Sensing, 47*(2–3), 145-161. doi: 10.1016/0924-2716(92)90030-d

ESA. (2005). SPARC-2004 Data Acquisition Report. In ESA (Ed.), (pp. 130). Valencia: European Spatial Agency.

Forsythe, K. W. (2006). Field Methods in Remote Sensing edited by Roger M. McCoy. *Canadian Geographer / Le Géographe canadien, 50*(4), 527-528. doi: 10.1111/j.1541-0064.2006.00161_2.x

Friedl, M. A. (2002). Forward and inverse modeling of land surface energy balance using surface temperature measurements. *Remote Sensing of Environment, 79*(2-3), 344-354. doi: 10.1016/s0034-4257(01)00284-x

Friedl, M. A., & Davis, F. W. (1994). Sources of variation in radiometric surface temperature over a tallgrass prairie. *Remote Sensing of Environment, 48*(1), 1-17. doi: 10.1016/0034-4257(94)90109-0

Gao, Z. Q., Zhang, W. J., Gao, W., & Chang, N. B. (2009). Modeling the land surface heat exchange process with the aid of moderate resolution imaging spectroradiometer images. *Journal of Applied Remote Sensing, 3*. doi: 033573

10.1117/1.3290811

Gibson, L. A., M¨unch Z., & J., E. (2011). Particular uncertainties encountered in using a pre-packaged SEBS model to derive evapotranspiration in a heterogeneous study area in South Africa. *Hydrol. Earth Syst. Sci., 15*, 295–310. doi: 10.5194/hess-15-295-2011

Godfray, H. C. J., Beddington, J. R., Crute, I. R., Haddad, L., Lawrence, D., Muir, J. F., . . . Toulmin, C. (2010). Food Security: The Challenge of Feeding 9 Billion People. *Science, 327*(5967), 812-818. doi: 10.1126/science.1185383

Jarvis, P. G. (1995). Scaling processes and problems. *Plant, Cell & Environment, 18*(10), 1079-1089. doi: 10.1111/j.1365-3040.1995.tb00620.x

Krishna, T., Ravikumar, G., & Krishnaveni, M. (2009). Remote sensing based agricultural drought assessment in Palar basin of Tamil Nadu state, India. *Journal of the Indian Society of Remote Sensing, 37*(1), 9-20. doi: 10.1007/s12524-009-0008-8

Lhomme, J.-P., Katerji, N., Perrier, A., & Bertolini, J.-M. (1988). Radiative surface temperature and convective flux calculation over crop canopies. *Boundary-Layer Meteorology, 43*(4), 383-392. doi: 10.1007/bf00121714

Lin, W. (2006). *Satellite based regional evapotransipiration in Hebei Plain North Eastern China.* MSc, International Institute of Geo-Information Science and Earth Observation, Enschede.

Liu, D., & Pu, R. (2008). Downscaling Thermal Infrared Radiance for Subpixel Land Surface Temperature Retrieval. *Sensors, 8*(4), 2695-2706.

Marshall, G., & Xiaobing, Z. (2004, 20-24 Sept. 2004). *Drought detection in semi-arid regions using remote sensing of vegetation indices and drought indices.* Paper presented at the Geoscience and Remote Sensing Symposium, 2004. IGARSS '04. Proceedings. 2004 IEEE International.

Mishra, A. K., & Singh, V. P. (2011). Drought modeling - A review. *Journal of Hydrology, 403*(1-2), 157-175. doi: 10.1016/j.jhydrol.2011.03.049

Norman, J. M., Divakarla, M., & Goel, N. S. (1995). Algorithms for extracting information from remote thermal-IR observations of the earth's surface. *Remote Sensing of Environment, 51*(1), 157-168. doi: 10.1016/0034-4257(94)00072-u

Olioso, A., Chauki, H., Courault, D., & Wigneron, J.-P. (1999). Estimation of Evapotranspiration and Photosynthesis by Assimilation of Remote Sensing Data into SVAT Models. *Remote Sensing of Environment, 68*(3), 341-356. doi: 10.1016/s0034-4257(98)00121-7

Ranson, K. J., Daughtry, C. S. T., Biehl, L. L., & Bauer, M. E. (1985). Sun-view angle effects on reflectance factors of corn canopies. *Remote Sensing of Environment, 18*(2), 147-161. doi: 10.1016/0034-4257(85)90045-8

Rao, V. R., Brach, E. J., & Mack, A. R. (1979). Bidirectional reflectance of crops and the soil contribution. *Remote Sensing of Environment, 8*(2), 115-125. doi: 10.1016/0034-4257(79)90012-9

Rasmussen, M. O., Pinheiro, A. C., Proud, S. R., & Sandholt, I. (2010). Modeling Angular Dependences in Land Surface Temperatures From the SEVIRI Instrument Onboard the Geostationary Meteosat Second Generation Satellites. *Geoscience and Remote Sensing, IEEE Transactions on, 48*(8), 3123-3133.

Rojas, O., Vrieling, A., & Rembold, F. (2011). Assessing drought probability for agricultural areas in Africa with coarse resolution remote sensing imagery. *Remote Sensing of Environment, 115*(2), 343-352. doi: 10.1016/j.rse.2010.09.006

Rosegrant, M. W., & Cline, S. A. (2003). Global Food Security: Challenges and Policies. *Science, 302*(5652), 1917-1919. doi: 10.1126/science.1092958

Shibayama, M., & Wiegand, C. L. (1985). View azimuth and zenith, and solar angle effects on wheat canopy reflectance. *Remote Sensing of Environment, 18*(1), 91-103. doi: 10.1016/0034-4257(85)90040-9

Su, Z. (1999). The Surface Energy Balance System (SEBS) for estimation of turbulent heat fluxes. [1999/11/30]. *Hydrol. Earth Syst. Sci., 6*(1), 16. doi: 0.5194/hess-6-85-2002

Valencia, G. U. o. (2011, July 29th). Overall description of the test site from http://www.uv.es/leo/scn2flex/site_description.htm

van der Kwast, J., Timmermans, W., Gieske, A., Su, Z., Olioso, A., Jia, L., . . . de Jong, S. (2009). Evaluation of the Surface Energy Balance System (SEBS) applied to ASTER imagery with flux-measurements at the SPARC 2004 site (Barrax, Spain)

JO - Hydrol. Earth Syst. Sci. *Hydrol. Earth Syst. Sci., 13*(7). doi: 10.5194/hess-13-1337-2009

Venus, V., & Rugege, D. (2004). Combined use of polar orbiting and geo - stationary satellites to improve time interpolation in dynamic crop models for food security assessment. *In: ISPRS 2004 : proceedings of the XXth ISPRS congress : Geo-imagery bridging continents, 12-23 July 2004, Istanbul, Turkey. Comm. VII PS, WG VII/2. pp. 212-219.*

Vonder, O. W., Clevers, J. G. P. W., Desprats, J. F., King, C., Prèvot, L., & Bruguier, N. (2000). Modelling Crop Geometry Using Multiple View Angles. *International Archives of Photogrammetry and Remote Sensing., XXXIII*(Part B7).

Wan, Z., Wang, P., & Li, X. (2004). Using MODIS Land Surface Temperature and Normalized Difference Vegetation Index products for monitoring drought in the southern Great Plains, USA. *International Journal of Remote Sensing, 25*(1), 61 - 72.

Weiss, M., Baret, F., Smith, G. J., Jonckheere, I., & Coppin, P. (2004). Review of methods for in situ leaf area index (LAI) determination: Part II. Estimation of LAI, errors and sampling. *Agricultural and Forest Meteorology, 121*(1–2), 37-53. doi: 10.1016/j.agrformet.2003.08.001

Wilhite, D., Svoboda, M., & Hayes, M. (2007). Understanding the complex impacts of drought: A key to enhancing drought mitigation and preparedness. *Water Resources Management, 21*(5), 763-774. doi: 10.1007/s11269-006-9076-5

Wilhite, D. A. (2007). Preparedness and Coping Strategies for Agricultural Drought Risk Management: Recent Progress and Trends. In M. V. K. Sivakumar & R. P. Motha (Eds.), *Managing Weather and Climate Risks in Agriculture* (pp. 21-38): Springer Berlin Heidelberg.

Wilson, T. B., & Meyers, T. P. (2007). Determining vegetation indices from solar and photosynthetically active radiation fluxes. *Agricultural and Forest Meteorology, 144*(3–4), 160-179. doi: 10.1016/j.agrformet.2007.04.001

Zhan, X., Kustas, W. P., & Humes, K. S. (1996). An intercomparison study on models of sensible heat flux over partial canopy surfaces with remotely sensed surface temperature. *Remote Sensing of Environment, 58*(3), 242-256. doi: 10.1016/s0034-4257(96)00049-1

APPENDICES

Appendix a: Aster data LAI calculations

Field	Operator	Coordinates		NDVI	Observed LAI	LAI_SEBS	Sqerror 1	BIAS	LAI model 2	Sqerror 2	BIAS
C1	A1	577799.4	4323405	0.651	1.85	1.7549	0.00904	0.0951	2.66907	0.67087	-0.81907
C1	F2	577737.6	4323396	0.634	1.58	1.6824	0.01049	-0.1024	2.50254	0.85108	-0.92254
C1	S1	577808.8	4323399	0.67	1.4	1.84136	0.1948	-0.4414	2.87769	2.18357	-1.47769
C1	U1	577807.9	4323406	0.651	1.76	1.7549	2.6E-05	0.0051	2.66907	0.8264	-0.90907
C1	U2	577728.3	4323394	0.639	1.72	1.70328	0.00028	0.01672	2.54979	0.68855	-0.82979
C3		579048.5	4323210	0.698	2.23	1.98104	0.06198	0.24896	3.2435	1.02718	-1.0135
C3		579159.8	4323123	0.715	2.47	2.07426	0.15661	0.39574	3.51337	1.08863	-1.04337
C5		578379.8	4324336	0.683	1.96	1.90424	0.00311	0.05576	3.03745	1.16091	-1.07745
C2		578110.5	4323589	0.723	3.1	2.12066	0.9591	0.97934	3.65758	0.3109	-0.55758
C2		578059.4	4323673	0.739	3.5	2.21897	1.64103	1.28103	3.99074	0.24083	-0.49074
G1	F1	577164.9	4324223	0.241	0.76	0.62773	0.0175	0.13227	0.57894	0.03278	0.181059
G1	F3	577093.5	4324174	0.263	0.72	0.67135	0.00237	0.04865	0.64358	0.00584	0.076417
G1	U2	577243.2	4324144	0.243	0.49	0.63167	0.02007	-0.1417	0.58471	0.00897	-0.09471
G1	U3	577440.3	4324071	0.291	0.63	0.72792	0.00959	-0.0979	0.72972	0.00994	-0.09972
V	V	577837.1	4323902	0.245	0.22	0.63562	0.17274	-0.4156	0.59051	0.13727	-0.37051
V	V	577793.9	4323918	0.272	0.31	0.68939	0.14393	-0.3794	0.67078	0.13016	-0.36078
V	V	577821.2	4323842	0.2	0.216	0.54772	0.11004	-0.3317	0.46488	0.06194	-0.24888
V	V	577841.3	4323794	0.181	0.256	0.51088	0.06497	-0.2549	0.4146	0.02515	-0.1586
V	V-red	577878.7	4323987	0.313	0.251	0.77344	0.27294	-0.5224	0.80073	0.3022	-0.54973
C1	C1-D1	577817.2	4323406	0.663	1.69	1.80879	0.01411	-0.1188	2.79771	1.22702	-1.10771
A1	A1-D1	574537.9	4326607	0.757	3.73	2.33954	1.93338	1.39046	4.47007	0.5477	-0.74007
A2	A2-D1	575359.6	4324909	0.736	3.36	2.19994	1.34573	1.16006	3.9229	0.31686	-0.5629
B1	B1-D1	574755	4325463	0.728	4.48	2.15057	5.42626	2.32943	3.75461	0.52618	0.725385
C9	C9-D1	575996	4326253	0.719	2.92	2.09725	0.67693	0.82275	3.58389	0.44075	-0.66389
C10	C10-D1	575970	4326580	0.71	2.57	2.04611	0.27446	0.52389	3.42929	0.73837	-0.85929
G1	G1-D1	577291	4324336	0.269	0.63	0.68336	0.00285	-0.0534	0.66166	0.001	-0.03166
G1	G1-D2	577248	4324376	0.278	0.63	0.70149	0.00511	-0.0715	0.68917	0.0035	-0.05917
G1	G1-D3	577207	4324386	0.273	0.63	0.6914	0.00377	-0.0614	0.67383	0.00192	-0.04383
G1	G1-D4	577580	4324213	0.27	0.63	0.68537	0.00307	-0.0554	0.6647	0.0012	-0.0347
P2	P2-D1	575755	4325413	0.656	3.96	1.77706	4.76521	2.18294	2.72145	1.53402	1.238555
P3	P3-D1	575030	4325513	0.687	4.03	1.92426	4.43414	2.10574	3.08992	0.88375	0.940082
SF1	SF1-D2	576298	4326203	0.513	0.5	1.26245	0.58133	-0.7624	1.64476	1.31047	-1.14476
A4	F1	573779	4327859	0.757	5.66	2.33954	11.0254	3.32046	4.47007	1.41593	1.189931
A4	F2	573753.2	4327822	0.742	3.41	2.23829	1.37291	1.17171	4.06152	0.42448	-0.65152
A4	U1	573719.6	4327838	0.754	4.01	2.31864	2.86071	1.69136	4.37981	0.13676	-0.36981
A4	U2	573661	4327795	0.749	3.52	2.28454	1.52636	1.23546	4.23961	0.51783	-0.71961
A5	F1	573467.9	4327715	0.762	5.25	2.37516	8.26473	2.87484	4.63251	0.38129	0.617486
A5	F2	573388.6	4327621	0.785	3.93	2.55291	1.89639	1.37709	5.7019	3.13963	-1.7719

G2	AT	574203.9	4326688	0.223	0.64	0.59245	0.00226	0.04755	0.52788	0.01257	0.112116
G2	A2	574333.1	4326759	0.235	0.078	0.61594	0.28938	-0.5379	0.56174	0.23401	-0.48374
G2	A3	574283.8	4326646	0.214	0.65	0.57492	0.00564	0.07508	0.50294	0.02163	0.14706
P1	A1	576661	4324722	0.693	5.29	1.95491	11.1229	3.33509	3.1719	4.48634	2.118098
P1	S1	576487.7	4324629	0.712	5.64	2.05729	12.8358	3.58271	3.4624	4.74192	2.177595
P1	S3	576625.7	4324717	0.693	5.89	1.95491	15.485	3.93509	3.1719	7.38806	2.718098
P1	S2	576506.2	4324571	0.698	5.97	1.98104	15.9118	3.98896	3.2435	7.4338	2.726499
P1	S4	576889.9	4324517	0.688	4.63	1.92932	7.2937	2.70068	3.1033	2.33081	1.5267
P1	S2	576796.7	4324486	0.642	4.16	1.71598	5.97323	2.44402	2.5788	2.50018	1.581196
C6	S1	577860.8	4324679	0.715	2.19	2.07426	0.0134	0.11574	3.51337	1.75132	-1.32337
C6	S2	577945.8	4324519	0.702	2.67	2.00235	0.44576	0.66765	3.30312	0.40084	-0.63312
P2	U1	575698.9	4325483	0.489	4.28	1.19369	9.52531	3.08631	1.51737	7.63215	2.762634
P2	U2	575616.5	4325439	0.649	4.72	1.74614	8.84384	2.97386	2.64857	4.29081	2.071426
P2	F1	575659.5	4325411	0.659	3.2	1.79056	1.98652	1.40944	2.7537	0.19919	0.446304
P2	F2	575611.3	4325382	0.656	3.65	1.77706	3.50789	1.87294	2.72145	0.86221	0.928555
						RMSE	**1.6455**	0.96852	**RMSE**	**1.12935**	0.038876

Appendix b: AHS LAI calculations

Field	**Operator**	**Coordinates**		**NDVI**	**SQerror1**	**LAI_model1**	**BIAS**	**Observed LAI**	**LAI_model2**	**Sqerror2**	**BIAS**
C1	A1	577799.4	4323404.5	0.751	0.20077	2.29807	-0.44807	1.85000	2.15901	0.09549	-0.30901
C1	F2	577737.6	4323395.6	0.723	0.29232	2.12066	-0.54066	1.58000	1.94561	0.13367	-0.36561
C1	S1	577808.8	4323399.4	0.707	0.39629	2.02952	-0.62952	1.40000	1.83923	0.19292	-0.43923
C1	U1	577807.9	4323405.8	0.748	0.26815	2.27783	-0.51783	1.76000	2.13418	0.14001	-0.37418
C1	U2	577728.3	4323393.9	0.741	0.26196	2.23182	-0.51182	1.72000	2.07823	0.12833	-0.35823
C3		579048.5	4323209.6	0.69	0.08440	1.93949	0.29051	2.23000	1.73593	0.24410	0.49407
C3		579159.8	4323122.7	0.705	0.20378	2.01858	0.45142	2.47000	1.82659	0.41398	0.64341
C5		578379.8	4324336.0	0.672	0.01192	1.85083	0.10917	1.96000	1.63573	0.10515	0.32427
C2		578110.5	4323588.8	0.761	0.53589	2.36795	0.73205	3.10000	2.24582	0.72962	0.85418
C2		578059.4	4323673.1	0.762	1.26528	2.37516	1.12484	3.50000	2.25487	1.55034	1.24513
G1	F1	577164.9	4324222.9	0.257	0.01012	0.65939	0.10061	0.76000	0.39622	0.13233	0.36378
G1	F3	577093.5	4324173.8	0.338	0.01135	0.82653	-0.10653	0.72000	0.55543	0.02708	0.16457
G1	U2	577243.	4324143.	0.176	0.00013	0.50118	-	0.49000	0.25621	0.05466	0.23379

		2	6				0.01118				
G1	U3	577440.3	4324071.4	0.209	0.00420	0.56519	0.06481	0.63000	0.31123	0.10161	0.31877
V	V	577837.1	4323902.1	0.175	0.07798	0.49924	-0.27924	0.22000	0.25458	0.00120	-0.03458
V	V	577793.9	4323917.7	0.228	0.08539	0.60222	-0.29222	0.31000	0.34413	0.00117	-0.03413
V	V	577821.2	4323842.4	0.172	0.07696	0.49342	-0.27742	0.21600	0.24971	0.00114	-0.03371
V	V	577841.3	4323793.7	0.185	0.06898	0.51864	-0.26264	0.25600	0.27096	0.00022	-0.01496
V	V-red	577878.7	4323986.8	0.247	0.15098	0.63956	-0.38856	0.25100	0.37800	0.01613	-0.12700
C1	C1-D1	577817.2	4323405.6	0.641	0.00047	1.71173	-0.02173	1.69000	1.48113	0.04363	0.20887
A1	A1-D1	574537.9	4326607.1	0.795	1.19161	2.63839	1.09161	3.73000	2.60156	1.27337	1.12844
A2	A2-D1	575359.6	4324909.0	0.789	0.59839	2.58644	0.77356	3.36000	2.53035	0.68832	0.82965
B1	B1-D1	574755.0	4325463.0	0.776	3.99825	2.48044	1.99956	4.48000	2.38956	4.36993	2.09044
C9	C9-D1	575996.0	4326253.0	0.789	0.11126	2.58644	0.33356	2.92000	2.53035	0.15183	0.38965
C10	C10-D1	575970.0	4326580.0	0.758	0.04991	2.34659	0.22341	2.57000	2.21909	0.12314	0.35091
G1	G1-D1	577291.0	4324336.0	0.285	0.00734	0.71568	-0.08568	0.63000	0.44883	0.03282	0.18117
G1	G1-D2	577248.0	4324376.0	0.278	0.00511	0.70149	-0.07149	0.63000	0.43545	0.03785	0.19455
G1	G1-D3	577207.0	4324386.0	0.261	0.00140	0.66735	-0.03735	0.63000	0.40359	0.05126	0.22641
G1	G1-D4	577580.0	4324213.0	0.264	0.00188	0.67334	-0.04334	0.63000	0.40915	0.04877	0.22085
P2	P2-D1	575755.0	4325413.0	0.691	4.06181	1.94461	2.01539	3.96000	1.74176	4.92057	2.21824
P3	P3-D1	575030.0	4325513.0	0.747	3.09354	2.27115	1.75885	4.03000	2.12602	3.62514	1.90398
SF1	SF1-D2	576298.0	4326203.0	0.493	0.49688	1.20490	-0.70490	0.50000	0.93870	0.19246	-0.43870
A4	F1	573779.0	4327858.6	0.82	7.73158	2.87943	2.78057	5.66000	2.95666	7.30806	2.70334
A4	F2	573753.2	4327822.3	0.794	0.60904	2.62959	0.78041	3.41000	2.58939	0.67340	0.82061
A4	U1	573719.6	4327837.8	0.814	1.42189	2.81757	1.19243	4.01000	2.86103	1.32013	1.14897
A4	U2	573661.0	4327794.8	0.808	0.58006	2.75838	0.76162	3.52000	2.77268	0.55849	0.74732

A5	F1	573467.9	4327715.2	0.806	6.30406	2.73921	2.51079	5.25000	2.74466	6.27675	2.50534
A5	F2	573388.6	4327620.5	0.797	1.62265	2.65617	1.27383	3.93000	2.62630	1.69962	1.30370
G2	AT	574203.9	4326688.1	0.159	0.02955	0.46810	0.17190	0.64000	0.22885	0.16905	0.41115
G2	A2	574333.1	4326759.3	0.172	0.08213	0.49342	0.28658	0.78000	0.24971	0.28121	0.53029
G2	A3	574283.8	4326646.4	0.161	0.03168	0.47201	0.17799	0.65000	0.23203	0.17470	0.41797
P1	A1	576661.0	4324721.9	0.691	11.19166	1.94461	3.34539	5.29000	1.74176	12.58998	3.54824
P1	S1	576487.7	4324629.1	0.708	12.99587	2.03502	3.60498	5.64000	1.84560	14.39748	3.79440
P1	S3	576625.7	4324716.6	0.724	14.16327	2.12659	3.76341	5.89000	1.95260	15.50314	3.93740
P1	S2	576506.2	4324570.5	0.737	14.16577	2.20626	3.76374	5.97000	2.04742	15.38661	3.92258
P1	S4	576889.9	4324516.5	0.685	7.37551	1.91421	2.71579	4.63000	1.70722	8.54263	2.92278
P1	S2	576796.7	4324486.2	0.633	6.15898	1.67827	2.48173	4.16000	1.44436	7.37473	2.71564
C6	S1	577860.8	4324679.3	0.789	0.15716	2.58644	-0.39644	2.19000	2.53035	0.11584	-0.34035
C6	S2	577945.8	4324519.3	0.753	0.12835	2.31175	0.35825	2.67000	2.17586	0.24417	0.49414
P2	U1	575698.9	4325483.1	0.681	5.69129	1.89436	2.38564	4.28000	1.68475	6.73531	2.59525
P2	U2	575616.5	4325438.5	0.7	7.44390	1.99165	2.72835	4.72000	1.79558	8.55224	2.92442
P2	F1	575659.5	4325411.4	0.599	2.73741	1.54549	1.65451	3.20000	1.29988	3.61045	1.90012
P2	F2	575611.3	4325382.0	0.612	4.22481	1.59457	2.05543	3.65000	1.35302	5.27610	2.29698
						RMSE	**0.83464**			**RMSE**	**1.00672**